Paper:
Sevilla, R. & Cottereau, R. (2018). Influence of periodically fluctuating material parameters on the stability of explicit high-order spectral element methods. *Journal of Computational Physics*
http://dx.doi.org/10.1016/j.jcp.2018.07.002

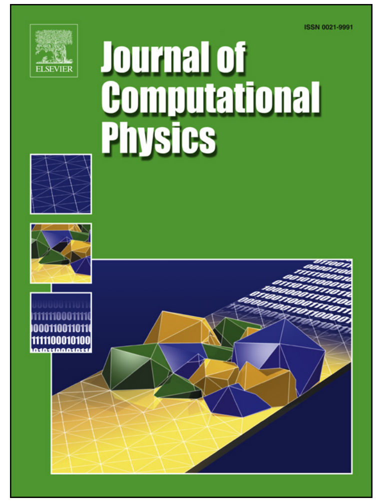

Influence of periodically fluctuating material parameters on the stability of explicit high-order spectral element methods

Ruben Sevilla, Régis Cottereau

PII: S0021-9991(18)30455-8
DOI: https://doi.org/10.1016/j.jcp.2018.07.002
Reference: YJCPH 8125

To appear in: *Journal of Computational Physics*

Received date: 22 April 2017
Revised date: 29 April 2018
Accepted date: 1 July 2018

Highlights

- Stability analysis of an explicit time marching algorithm for the spectral element method in heterogeneous media.
- The origin of instabilities that are often observed when the stability limit derived for homogeneous materials is adapted is revealed.
- Numerical examples show that adapting homogeneous formulae for heterogeneous media leads to either instability or to unnecessary increased computational resources.
- Extensions of the results derived for quadratic and cubic one dimensional spectral elements are discussed, including higher order approximations, different periodicity of the material parameters and higher dimensions.
- Numerical experiments reveal that the stability limits derived for periodically fluctuating material properties are precise when the material parameters take the same value at the vertices of the mesh even for non-periodic fluctuations.

Influence of periodically fluctuating material parameters on the stability of explicit high-order spectral element methods

Ruben Sevilla*

Zienkiewicz Centre for Computational Engineering, College of Engineering, Swansea University, Swansea, SA1 8EN, Wales, UK.

Régis Cottereau

MSSMat, CNRS, CentraleSupélec, Université Paris-Saclay, France

Abstract

This paper aims at studying the influence of material heterogeneity on the stability of explicit time marching schemes for the high-order spectral element discretisation of wave propagation problems. A periodic fluctuation of the density and stiffness parameters is considered, where the period is related to the characteristic element size of the mesh. A new stability criterion is derived analytically for quadratic and cubic one-dimensional spectral elements in heterogeneous materials by using a standard Von Neumann analysis. The analysis presented illustrates the effect of material heterogeneity on the stability limit and also reveals the origin of instabilities that are often observed when the stability limit derived for homogeneous materials is adapted by simply changing the velocity of the wave to account for the material heterogeneity. Several extensions of the results derived for quadratic and cubic one-dimensional spectral elements are discussed, including higher order approximations, different periodicity of the material parameters and higher dimensions. Extensive numerical results demonstrate the validity of the new stability limits derived for heterogeneous materials with periodic fluctuation. Finally numerical examples of the

*Corresponding author
Email address: `r.sevilla@swansea.ac.uk` (Ruben Sevilla)

stability for randomly fluctuating material properties are also presented, discussing the applicability of the theoretical limits derived for material properties with periodic fluctuation.

Keywords: spectral element method, explicit time integration, stability, heterogeneous media, high-order

1. Introduction

Explicit time marching schemes for high-order spectral element discretisations of wave propagation problems are known to be conditionally stable [1]. For a homogeneous one-dimensional problem with constant element size, the stability criterion is given by

$$\alpha = \frac{c\Delta t}{h} \leq \alpha_M, \tag{1}$$

where c is the wave velocity, Δt is the time step, and h is the characteristic element size. The stability limit, α_M, is a scalar that depends upon the polynomial order p and the dimensionality of the problem d. Its value can be derived analytically for homogeneous media [1, 2, 3, 4, 5]. Table 1 summarises the values for polynomial approximations up to order $p = 5$ when the spectral element method is combined with the Leap-Frog time marching scheme. For regular meshes in d dimensions, the value of the stability limit is simply that for one-dimensional problems divided by $\sqrt{d}$.

Table 1: Approximate value of the stability limit α_M for spectral elements of polynomial order p with the Leap-Frog scheme assuming a regular mesh and constant wave velocity.

$p =$	1	2	3	4	5
1D	1.00	0.40	0.23	0.14	0.10
2D	0.70	0.28	0.16	0.10	0.07
3D	0.57	0.23	0.13	0.08	0.05

The results in Table 1 are derived for homogeneous material parameters and regular meshes. Numerical tests showing the negative influence of the deformation of the elements on the stability are reported in [1]. Some hints can also be found about the error induced by the presence of a discontinuity or heterogeneity of the material properties [6, 7, 1], but no general stability criteria exists in that case. A rule of thumb extending Equation (1) is typically applied, in which (i) the polynomial order is indirectly taken into account by choosing h as the smallest distance between two interpolation points in an element, (ii) element-wise maximum, average, or local value of the velocity $c(x)$ is chosen, and (iii) a heuristic value of the stability criteria α_M is considered. Most authors (see for instance [8, 9, 10]) choose a stability criterion close to 0.3-0.4, but it can go as high as 0.6 [11, 12], or as low as 0.07 for non-conforming meshes [13] (with a discontinuous Galerkin approach). As with any heuristic criterion, the risk is either to run into unstable cases by considering a high value or to waste computational resources by employing a low value.

This paper aims at describing the influence of material heterogeneity on the stability of explicit time marching schemes for the high-order spectral element discretisation of wave propagation problems. A periodic fluctuation of the density and stiffness parameters is considered, whose period is related to the characteristic element size h. A classical Von Neumann stability analysis is performed for quadratic and cubic spectral elements in one dimension. This analysis not only provides an analytical stability limit but also demonstrates that a heuristic approach can lead to unstable simulations or to unnecessary expensive simulations when the stability limit derived for the homogeneous case is adapted by simply changing the velocity of the wave to account for the material heterogeneity. It is worth noting that this is true even for relative low orders of approximation (e.g. $p = 2$). Several extensions of the results derived for quadratic and cubic one-dimensional spectral elements are discussed, including higher order approximations, different periodicity of the material parameters and higher dimensions. A number of numerical examples are presented to show the validity of the stability limits obtained. These values are also compared with the stability limits that would be derived from the results available in the literature for homogeneous materials. Finally, the paper presents several numerical examples to discuss the validity of the stability limits obtained for periodically fluctuating material properties when applied to problems with randomnly fluctuating material properties.

2. Problem statement and discretisation

2.1. Weak formulation

Let us consider the one-dimensional acoustic wave equation in a heterogeneous medium Ω characterised by a density function $\eta(x)$ and a Lamé parameter $\gamma(x)$,

$$\eta(x)\frac{\partial^2 u(x,t)}{\partial t^2} - \frac{\partial}{\partial x}\left(\gamma(x)\frac{\partial u(x,t)}{\partial x}\right) = f(x,t), \quad \text{for } (x,t) \in \Omega \times (0,T], \tag{2}$$

where $u(x,t)$ is a scalar field, $f(x,t)$ denotes a time-dependent external force and T denotes the final time. The problem is closed by considering appropriate initial and boundary conditions, namely

$$u(x,0) = u_0(x), \qquad \frac{\partial u(x,0)}{\partial t} = v_0(x), \qquad \text{for } x \in \Omega. \tag{3}$$

and

$$u(x,t) = u_d(t), \quad \text{for } x \in \partial\Omega \times (0,T], \tag{4}$$

where, to simplify the presentation, only Dirichlet boundary conditions are considered.

The weak statement equivalent to the strong form (2), is obtained by multiplying Equation (2) by a test function $w(x)$, integrating in the whole domain and performing an integration by parts of the term with second order spatial derivatives. The resulting weak form reads: find $u(x,t) \in \mathcal{W}_t$ such that $u(x,t) = u_d(t)$ on $\partial\Omega \times [0,T]$ and

$$\int_\Omega \eta(x)w(x)\frac{\partial^2 u(x,t)}{\partial t^2}dx + \int_\Omega \gamma(x)\frac{\partial w(x)}{\partial x}\frac{\partial u(x,t)}{\partial x}dx = \int_\Omega w(x)f(x,t)dx, \tag{5}$$

for all $w(x) \in \mathcal{H}^1_0(\Omega)$, where

$$\mathcal{W}_t = \left\{ u \mid u(\cdot,t) \in \mathcal{H}^1(\Omega), t \in [0,T] \text{ and } u(x,t) = u_d(x,t) \text{ for } (x,t) \in \partial\Omega \times [0,T] \right\}. \tag{6}$$

2.2. Spatial and temporal discretisation

The spatial domain is discretised in elements $\Omega_i = [x_i, x_{i+1}]$ and a nodal approximation of the solution is considered within each element using the Gauss-Lobatto-Legendre (GLL) points, denoted by $\{x_i, x_{i,1}, \ldots, x_{i,p-1}, x_{i+1}\}$. The first and last GLL points within an element correspond to the vertices, x_i and x_{i+1}, respectively. The approximate solution within an element Ω_i, $u_h^i = u_{h|\Omega_i}$, is given by

$$u_h^i(x,t) = N_i(x)U_i(t) + N_{i+1}(x)U_{i+1}(t) + \sum_{j=1}^{p-1} N_{i,j}(x)U_{i,j}(t), \tag{7}$$

where $\{N_i, N_{i,1}, \ldots, N_{i,p-1}, N_{i+1}\}$ are Lagrange polynomials of degree p and $\{U_i, U_{i,1}, \ldots, U_{i,p-1}, U_{i+1}\}$ denote the time-dependent values of the solution at the nodal points.

Introducing the approximation of the solution in the weak formulation of Equation (5) and selecting the space of the weighting functions to be the same as the space of the interpolation functions, leads to the semi-discrete system of ordinary differential equations

$$\mathbf{M}\frac{d^2\mathbf{U}}{dt^2} + \mathbf{K}\mathbf{U} = \mathbf{F}, \tag{8}$$

where the mass matrix $\mathbf{M}$, the stiffness matrix $\mathbf{K}$ and the forcing vector $\mathbf{F}$ are given by

$$M_i^j = \int_\Omega \eta N_i N_j d\Omega, \qquad K_i^j = \int_\Omega \gamma \frac{\partial N_i}{\partial x}\frac{\partial N_j}{\partial x} d\Omega, \qquad F_i = \int_\Omega N_i f d\Omega \tag{9}$$

and computed by assembling the elemental contributions.

The integrals are computed using a numerical quadrature defined over the reference element. In a standard finite element method, Gauss-Legendre quadratures are considered, providing the highest order possible for a given set of integration points. However, this formulation leads to a dense global mass matrix.

In the so-called *spectral element method* (SEM) [14, 15], the quadrature points are selected to be the same as the nodal points (i.e. the GLL distribution), leading to a diagonal global mass matrix.

The main benefit of the SEM is its efficiency when combined with an explicit time marching algorithm. In this work, the classical second-order accurate Leap-Frog scheme is considered. At each time step, the solution is advanced in time according to

$$\mathbf{U}^{n+1} = 2\mathbf{U}^{n} - \mathbf{U}^{n-1} + \Delta t^2 \mathbf{M}^{-1} \left(\mathbf{F}^{n} - \mathbf{K}\mathbf{U}^{n} \right), \tag{10}$$

where it is worth emphasising that, in the context of the SEM, each time step only involves the solution of a trivial system of equations with diagonal mass matrix.

3. Stability analysis for quadratic spectral elements

In this section, the model problem of Equation (2) is considered in $\Omega = \mathbb{R}$ with no external forces and the classical Von Neumann stability analysis is performed for the SEM with quadratic elements. A one-dimensional uniform mesh is considered where the element size is defined as

$$h = x_{i+1} - x_i, \quad \forall i \in \mathbb{Z} \tag{11}$$

and the material properties are considered periodic, with period equal to the element size h, that is

$$\gamma(x) = \gamma(x + rh) \quad \text{and} \quad \eta(x) = \eta(x + rh), \quad \forall x \in \Omega, \quad \forall r \in \mathbb{Z}. \tag{12}$$

3.1. Dispersion relations

The SEM produces the following semi-discrete equations

$$M_i^i \frac{d^2 U_i}{dt^2} + \left(K_{i-1}^i U_{i-1} + K_{i-1,1}^i U_{i-1,1} + K_i^i U_i + K_{i,1}^i U_{i,1} + K_{i+1}^i U_{i+1} \right) = 0, \tag{13}$$

$$M_{i,1}^{i,1} \frac{d^2 U_{i,1}}{dt^2} + \left(K_i^{i,1} U_i + K_{i,1}^{i,1} U_{i,1} + K_{i+1}^{i,1} U_{i+1} \right) = 0, \tag{14}$$

for a vertex and an interior node of a quadratic element respectively where, using the corresponding GLL quadrature points, the terms of the mass and stiffness matrix are given by

$$M_i^i = \frac{h}{3}\eta_i, \qquad M_{i,1}^{i,1} = \frac{2h}{3}\eta_{i,1}, \qquad K_i^i = \frac{2}{3h}\left(5\gamma_i + \gamma_{i,1}\right), \qquad K_{i,1}^{i,1} = \frac{16}{3h}\gamma_i, \tag{15}$$

$$K_{i-1,1}^i = K_{i,1}^i = K_i^{i,1} = -\frac{8}{3h}\gamma_i, \qquad K_{i-1}^i = K_{i+1}^i = \frac{1}{3h}\left(3\gamma_i - 2\gamma_{i,1}\right). \tag{16}$$

Assuming plane wave solutions

$$U_i = \alpha_1 e^{I(ikh - w_h t)} \qquad U_{i,1} = \alpha_2 e^{I([i+1/2]kh - w_h t)}, \tag{17}$$

with $I = \sqrt{-1}$, Equations (13) and (14) lead to the following generalised eigenvalue problem

$$\widehat{\mathbf{K}} \begin{pmatrix} \alpha_1 \\ \alpha_2 \end{pmatrix} = w_h^2 \widehat{\mathbf{M}} \begin{pmatrix} \alpha_1 \\ \alpha_2 \end{pmatrix} \tag{18}$$

where

$$\widehat{\mathbf{K}} = \begin{pmatrix} 2\cos(kh)K_{i+1}^i + K_i^i & K_{i-1,1}^i e^{-Ikh/2} + K_{i,1}^i e^{Ikh/2} \\ K_{i,1}^i e^{-Ikh/2} + K_{i-1,1}^i e^{Ikh/2} & K_{i,1}^{i,1} \end{pmatrix} \tag{19}$$

and

$$\widehat{\mathbf{M}} = \begin{pmatrix} M_i^i & 0 \\ 0 & M_{i,1}^{i,1} \end{pmatrix}. \tag{20}$$

The characteristic equation of the generalised eigenvalue problem (18) is

$$\left(\frac{hw_h}{c_\star}\right)^4 - 4\left(6\beta^2 - \delta\omega^2\right)\left(\frac{hw_h}{c_\star}\right)^2 + 96\beta^2\omega^2 = 0, \tag{21}$$

with

$$c_\star^2 = \frac{\gamma_i + 2\gamma_{i,1}}{\eta_i + 2\eta_{i,1}}, \quad \beta^2 = \frac{1}{c_\star^4}\frac{\gamma_i(\gamma_i + 2\gamma_{i,1})}{3\eta_i\eta_{i,1}}, \quad \delta = \frac{1}{c_\star^2}\frac{3\gamma_i - 2\gamma_{i,1}}{\eta_i}, \quad \omega = \sin(kh/2). \tag{22}$$

The parameter $c_\star$ has units of velocity whereas $\beta > 0$, δ and ω are dimensionless. The parameter δ may be positive or negative, depending on the sign of $3\gamma_i - 2\gamma_{i,1}$. The homogeneous case ($\gamma_i = \gamma_{i,1}$ and $\eta_i = \eta_{i,1}$) corresponds to $\beta = \delta = 1$ and $c_\star^2 = \gamma_i/\eta_i = \gamma_{i,1}/\eta_{i,1}$.

It is worth mentioning that the velocity $c_\star$ corresponds to the approximation of $\sqrt{\int_{\Omega_i}\gamma(x)/\int_{\Omega_i}\eta(x)}$ by using the GLL quadrature with three integration points.

The roots of the characteristic polynomial of Equation (21) are

$$w_{h,1}^2 = 2\left(\frac{c_\star}{h}\right)^2\left((6\beta^2-\delta\omega^2)-\sqrt{(6\beta^2-\delta\omega^2)^2-24\beta^2\omega^2}\right), \tag{23}$$

$$w_{h,2}^2 = 2\left(\frac{c_\star}{h}\right)^2\left((6\beta^2-\delta\omega^2)+\sqrt{(6\beta^2-\delta\omega^2)^2-24\beta^2\omega^2}\right), \tag{24}$$

which reduce to the roots of the homogeneous case considered in [1] when $\beta = \delta = 1$.

The Taylor series expansion of the two roots leads to

$$w_{h,1}^2 = c_\star^2 k^2\left[1+\frac{1+\delta-2\beta^2}{24\beta^2}k^2h^2+\mathcal{O}(k^4h^4)\right], \tag{25}$$

$$w_{h,2}^2 = c_\star^2 k^2\left[\frac{24\beta^2}{k^2h^2}-(1+\delta)-\frac{1}{24\beta^2}(1+\delta)(1-2\beta^2)k^2h^2+\mathcal{O}(k^4h^4)\right], \tag{26}$$

where it can be observed that Equation (25) corresponds to an approximation of the dispersion relation of the wave equation whereas Equation (26) corresponds to a parasitic wave.

It is worth noting that the particular case of a medium with $\delta - 2\beta^2 = 1$ induces a superconvergent phenomenon as the Taylor expansion of Equation (25) is of order four. Superconvergence has been previously reported for homogeneous medium [1] but the analysis presented here shows that this behaviour can also be obtained for a heterogeneous medium. However, it is important to note that the objective of the Taylor expansion of the roots is to distinguish the parasitic wave from the physical wave rather than to extract any conclusions about the accuracy of the roots as the element size h tends to zero.

3.2. Stability for the Leap-Frog scheme

The dispersion relations for the SEM with a Leap-Frog time integrator are given by

$$\frac{4}{\Delta t^2}\sin^2\left(\frac{w_{h,l}^2\Delta t}{2}\right) = w_{h,l}^2, \quad \text{for } l = 1,2. \tag{27}$$

The stability of the discrete scheme is controlled by the conditions $w_{h,l}^2 \Delta t^2 \leq 4$ for $l = 1, 2$, that is

$$\sqrt{\max_{l=1,2} \left\{ \sup_{\omega \in [-1,1]} w_{h,l}^2(\omega), 0 \right\}} \leq \frac{2}{\Delta t}. \tag{28}$$

The supremum of the roots is found by studying the zeros of $\partial w_{h,l}^2 / \partial \omega$ for $l = 1, 2$. Firstly, $\partial w_{h,1}^2 / \partial \omega$ only vanishes if $\delta = -1$ or $\omega = 0$. If $\delta = -1$, $w_{h,1}^2 = 4c_\star^2 \omega^2 / h^2$, whose maximum is $4c_\star^2/h^2$. Otherwise, the supremum is attained for $\omega = 0$ or in the bounds of the interval, namely $\omega = -1$ and $\omega = 1$. Observing that $w_{h,1}^2(-1) = w_{h,1}^2(1) = 2c_\star^2(6\beta^2 - \delta - \sqrt{(6\beta^2 - \delta)^2 - 24\beta^2})/h^2$, leads to (the second value includes the maximum obtained for the special case when $\delta = -1$)

$$\sup_{\omega \in [-1,1]} w_{h,1}^2(\omega) = 2\frac{c_\star^2}{h^2} \max\left\{0, 6\beta^2 - \delta - \sqrt{(6\beta^2 - \delta)^2 - 24\beta^2}\right\}. \tag{29}$$

Secondly, $\partial w_{h,2}^2 / \partial \omega$ only vanishes when $\delta = -1$ or $\omega = 0$. If $\delta = -1$, the roots takes a constant value $w_{h,2}^2 = 24(\beta c_\star / h)^2$. Otherwise, observing that $w_{h,2}^2(0) = 24(\beta c_\star/h)^2$ and that at the bounds of the interval $w_{h,2}^2(-1) = w_{h,2}^2(1) = 2c_\star^2(6\beta^2 - \delta + \sqrt{(6\beta^2 - \delta)^2 - 24\beta^2})/h^2$, leads to

$$\sup_{\omega \in [-1,1]} w_{h,2}^2(\omega) = 2\frac{c_\star^2}{h^2} \max\left\{12\beta^2, 6\beta^2 - \delta + \sqrt{(6\beta^2 - \delta)^2 - 24\beta^2}\right\}. \tag{30}$$

The stability condition is therefore given by

$$\alpha = \frac{c_\star \Delta t}{h} \leq \alpha_M, \tag{31}$$

with

$$\alpha_M := \min\left\{ \frac{\sqrt{6}}{6\beta}, \sqrt{\frac{2}{6\beta^2 - \delta + \sqrt{(6\beta^2 - \delta)^2 - 24\beta^2}}} \right\}. \tag{32}$$

It can be observed that the well known homogeneous stability condition $\alpha_M = 1/\sqrt{6} \approx 0.40$ (see Table 1) is recovered when $\beta = \delta = 1$.

3.3. Discussion

The positivity of the polynomial function $P(\beta, \delta) = (6\beta^2 - \delta\omega^2)^2 - 24\beta^2\omega^2$ is discussed next as the square root of this function appears in the stability constant of Equation (32). It is worth noting that the parameters β and δ can be expressed as a function of the ratios $Q_\gamma = \gamma_{i,1}/\gamma_i$ and $Q_\eta = \eta_{i,1}/\eta_i$ and the velocity $c_\star$ can be expressed as a function of Q_γ, Q_η and the ratio $c_i^2 = \gamma_i/\eta_i$ as

$$\beta^2 = \frac{(1+2Q_\eta)^2}{3Q_\eta(1+2Q_\gamma)}, \qquad \delta = (3-2Q_\gamma)\frac{1+2Q_\eta}{1+2Q_\gamma}, \qquad c_\star^2 = c_i^2\frac{1+2Q_\gamma}{1+2Q_\eta}. \tag{33}$$

Rewriting the polynomial as a function of the ratios of the material properties leads to

$$\frac{Q_\eta^2(1+2Q_\gamma)^2}{(1+2Q_\eta)^2}P(Q_\gamma,Q_\eta) = \big(2(1+2Q_\eta) - Q_\eta\omega^2(3-2Q_\gamma)\big)^2 - 8Q_\eta\omega^2(1+2Q_\gamma), \tag{34}$$

and by considering the right-hand side function as a polynomial in Q_γ with positive leading term, its minimum is attained at $Q_\gamma = (2-4Q_\eta+3Q_\eta\omega^2)/(2Q_\eta\omega^2)$. After simplification, the minimum is obtained as

$$\min_{Q_\gamma} \frac{Q_\eta^2(1+2Q_\gamma)^2}{(1+2Q_\eta)^2}P(Q_\gamma,Q_\eta) = 32Q_\eta(1-\omega^2). \tag{35}$$

As $\omega^2 \in [0,1]$, the minimum is always positive and it is attained for $\omega^2 = 1$. Therefore, it is concluded that $P(\beta,\delta) \geq 0$ for all Q_γ and Q_η.

Finally, as $6\beta^2 - \delta$ is proportional to $2 + Q_\eta + 6Q_\eta Q_\gamma$ it is clear that $6\beta^2 - \delta + \sqrt{P(\beta,\delta)} \geq 0$, so the stability constant α_M of Equation (32) is always a real number.

The analysis presented in the previous section not only shows the stability condition for the periodic heterogeneous media considered. More importantly, it explains why the stability limit derived from the homogeneous case can lead to either inefficient simulations or to instabilities if applied to a problem with heterogeneous material properties. In the absence of theoretical results for heterogeneous media, a possible choice for the time step would be to consider the value of α_M of the homogeneous case and the maximum value of the nodal wave velocities [16, 17], that is

$$\Delta t = \frac{h}{\max_i\{c_i\}\sqrt{6}}. \tag{36}$$

However, contrary to the homogeneous case, in the heterogeneous case the supreme of $w_{h,2}$ is not always attained at $\omega = 0$. To illustrate the effect of

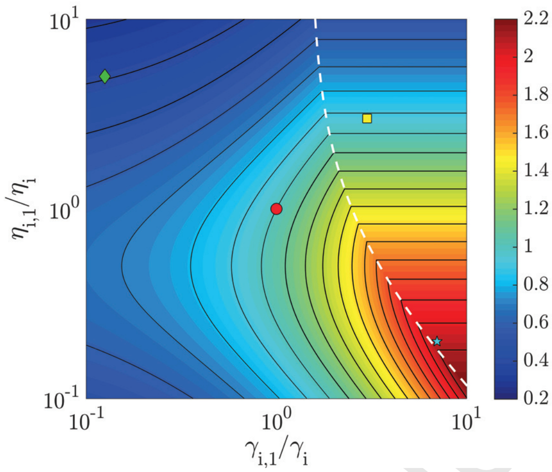

Figure 1: Ratio between the value of α_M for the heterogeneous and homogeneous cases for different values of the ratios $Q_\gamma = \gamma_{i,1}/\gamma_i$ and $Q_\eta = \eta_{i,1}/\eta_i$. The red dot indicates the homogeneous case and the white discontinuous line represents the change of definition of α_M given by maximum in Equation (31). The other symbols correspond to the numerical experiments presented in Section 3.4.

the heterogeneity in the stability limit, Figure 1 shows the ratio between the value of α_M for the heterogeneous and homogeneous cases for different values of the ratios Q_γ and Q_η. When the ratio between the value of α_M for the heterogeneous and homogeneous cases is lower than one, the expression of Equation (36) will lead to unstable results. In contrast, when the ratio is higher than one, using Equation (36) will result in an unnecessary increased computational cost. It is important to emphasise that depending upon the fluctuation of the material parameters, the value of α_M for the heterogeneous and homogeneous cases can differ significantly. For a fluctuation up to one order of magnitude in the values of γ and η, the ratio between the value of α_M for the heterogeneous and homogeneous cases varies between 0.2 and 2.2 as shown in Figure 1. The discontinuous line in Figure 1 denotes the change of definition in the maximum appearing in the denominator of Equation (32), which corresponds to $\delta = -1$ or, equivalently, to $Q_\eta(2Q_\gamma - 3) = 2$.

Interestingly, this figure can also be used as a guide for generating the computational mesh. Indeed, the strong asymmetry between the values of the parameters in the middle of the elements and at the vertices means that it is preferable to mesh the domain with elements such that the low values of the parameter $\eta(x)$ and the high values of the parameter $\gamma(x)$ fall in the middle of the elements. In particular, for periodic materials and meshes, it is always possible to translate the mesh, and therefore to move around in Figure 1 so as to optimise the time step. Note that such a translation would also impact the accuracy, which is not considered here.

3.4. Numerical examples

Three numerical examples are presented to validate the stability condition derived in this Section and to illustrate that using a condition derived for the homogeneous case can lead to either unstable results or inefficient computations. The domain $\Omega = [0, 1]$ is considered and the material parameters are defined as

$$\gamma(x) = \gamma_i + (\gamma_{i,1} - \gamma_i)\sin^2(\pi x/h), \qquad \eta(x) = \eta_i + (\eta_{i,1} - \eta_i)\sin^2(\pi x/h), \quad (37)$$

where both functions are defined in terms of the values of the material parameter at the vertices (γ_i and η_i) and at the interior nodes ($\gamma_{i,1}$ and $\eta_{i,1}$).

The analytical solution is given by

$$u(x, t) = \cos(2\pi t)\sin(2\pi x) \quad (38)$$

and the initial, boundary conditions and source term are derived from the exact solution as usually done in the method of manufactured solutions. In all the examples, the solution is advanced in time up to a final time $T = 10$ and the relative error in the $\mathcal{L}^2(\Omega)$ norm is measured. It is worth emphasising that the objective of the numerical examples is not to evaluate the accuracy of the numerical scheme but the accuracy of the stability limit derived for quadratic spectral elements with a periodic fluctuation of the material properties.

The first example considers $\gamma_i = 1$, $\gamma_{i,1} = 3$, $\eta_i = 1$ and $\eta_{i,1} = 3$. The stability condition given by Equation (32) is $\alpha_M = 1/\sqrt{7} \approx 0.37796$. Figure 2 (a) shows the relative error in the $\mathcal{L}^2(\Omega)$ norm as a function of the value of α

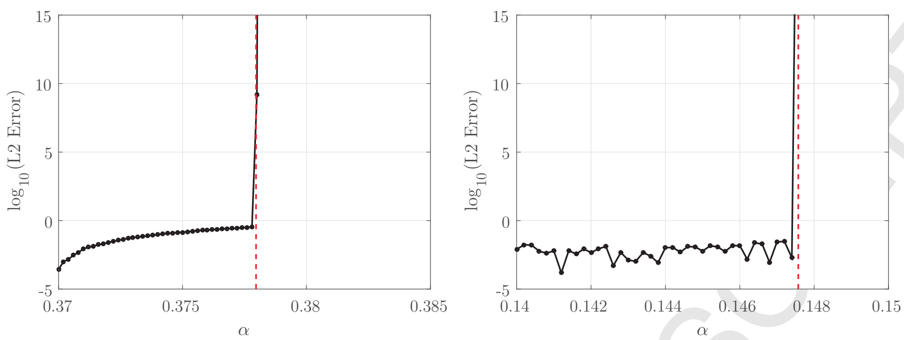

(a) (b)

Figure 2: Relative error in the $\mathcal{L}^2(\Omega)$ norm as a function of $\alpha = c_\star \Delta t/h$ for (a) $Q_\gamma = 3, Q_\eta = 3$ and (b) $Q_\gamma = 7, Q_\eta = 1/5$. The discontinuous line represents the stability limit corresponding to α_M.

considered to define the time step Δt for a uniform mesh with $h = 0.01$. It can be clearly observed that when the time step is defined by using a value of $\alpha \leq \alpha_M$ stability is guaranteed, whereas a value of $\alpha > \alpha_M$ leads to unstable results. More precisely, a value of $\alpha = 0.378$ (i.e, $\Delta t \approx 3.78 \times 10^{-3}$) leads to an instability, with a final error of 6.1×10^7 whereas a value of $\alpha = 0.37795$ (i.e, $\Delta t \approx 3.7795 \times 10^{-3}$) leads to stable results, with a final error of 3.77×10^{-4}. In this example, if the time step is computed using the results derived from the homogeneous case, as detailed in Equation (36), the result is $\Delta t \approx 4.08 \times 10^{-3}$, clearly leading to unstable results.

The next example considers a higher fluctuation in the material properties, namely $\gamma_i = 1$, $\eta_i = 5$, $\gamma_{i,1} = 7$ and $\eta_{i,1} = 1$. The stability condition given by Equation (32) is $\alpha_M = 7\sqrt{10}/150 \approx 0.14757$. Figure 2 (b) shows the relative error in the $\mathcal{L}^2(\Omega)$ norm as a function of the value of α considered to define the time step Δt for a uniform mesh with $h = 0.01$. As in the previous example, it can be clearly observed that the stability derived in this section holds.

The previous examples considered material parameters such that the minimum in Equation (32) is achieved by the first term, i.e. $\alpha_M = 1/(\beta\sqrt{6})$. The last example considers $\gamma_i = 8$, $\eta_i = 1$, $\gamma_{i,1} = 5$ and $\eta_{i,1} = 1$. The pa-

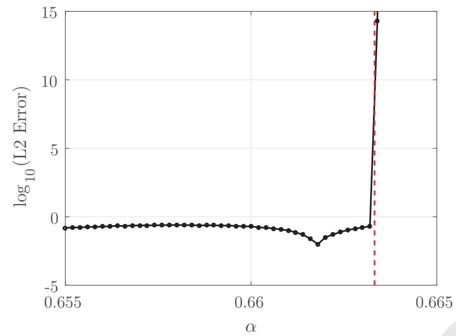

Figure 3: Relative error in the $\mathcal{L}^2(\Omega)$ norm as a function of $\alpha = c_\star \Delta t/h$ for $\gamma_i = 8$, $\eta_i = 1$, $\gamma_{i,1} = 5$ and $\eta_{i,1} = 1$. The discontinuous line represents the stability limit corresponding to α_M.

rameters have been selected to ensure that the minimum in Equation (32) is achieved by the second term in Equation (32). The value of the stability limit is $\alpha_M = \sqrt{11}/5 \approx 0.66332$. As in previous examples, Figure 3 shows the relative error in the $\mathcal{L}^2(\Omega)$ norm as a function of the value of α considered to define the time step Δt for a uniform mesh with $h = 0.01$. The results demonstrate the validity of the stability limit derived in this section. As in the first example, if the value of the stability limit given by the homogeneous case is considered unstable results are obtained.

4. Stability analysis for cubic spectral elements

This Section presents the classical Von Neumann stability analysis for the SEM with cubic elements for the model problem of Equation (2). Analogously to the quadratic case, a one-dimensional uniform mesh is considered and the material properties are assumed periodic, with period equal to the element size.

4.1. Dispersion relations

Following the procedure presented in Section 3.1, the characteristic equation of the generalised eigenvalue problem for cubic spectral elements is

$$\left(\frac{hw_h}{c_\star}\right)^6 - 2(2\delta_1\omega^2 + 45A_1)\left(\frac{hw_h}{c_\star}\right)^4 + 120(15\beta^2 - 2\delta_2\omega^2)\left(\frac{hw_h}{c_\star}\right)^2 - 7200\beta^2\omega^2 = 0, \tag{39}$$

with

$$c_\star^2 = \frac{36\gamma_i(\gamma_i\gamma_{i,1} + 2\gamma_{i,1}\gamma_{i,2} + \gamma_{i,2}\gamma_i)}{(5\gamma_i^2 + 3\gamma_i\gamma_{i,1} + \gamma_{i,1}\gamma_{i,2} + 3\gamma_{i,2}\gamma_i)(2\eta_i + 5\eta_{i,1} + 5\eta_{i,2})}, \tag{40}$$

$$\beta^2 = \frac{1}{4c_\star^6}\frac{\gamma_i(\gamma_i\gamma_{i,1} + 2\gamma_{i,1}\gamma_{i,2} + \gamma_{i,2}\gamma_i)}{\eta_i\eta_{i,1}\eta_{i,2}}, \tag{41}$$

$$A_1 = \frac{1}{18c_\star^2}\left(\frac{3\gamma_i + \gamma_{i,1}}{\eta_{i,2}} + \frac{3\gamma_i + \gamma_{i,2}}{\eta_{i,1}} + \frac{5}{2}\frac{2\gamma_i + \gamma_{i,1} + \gamma_{i,2}}{\eta_i}\right), \tag{42}$$

$$\delta_1 = \frac{1}{c_\star^2}\frac{12\gamma_i - 5\gamma_{i,1} - 5\gamma_{i,2}}{2\eta_i}, \tag{43}$$

$$\delta_2 = 30\frac{(\eta_{i,1} + \eta_{i,2})\beta^2}{(2\eta_i + 5\eta_{i,1} + 5\eta_{i,2})} - \frac{1}{4c_\star^4}c_i^2\left(\frac{\gamma_i + 7\gamma_{i,1}}{\eta_{i,2}} + \frac{\gamma_i + 7\gamma_{i,2}}{\eta_{i,1}}\right). \tag{44}$$

The parameter $c_\star$ has units of velocity while $\beta > 0$, $A_1 > 0$, δ_1, δ_2 and ω are dimensionless. The parameters δ_1 and δ_2 may be positive or negative. The homogeneous case ($\gamma_i = \gamma_{i,1} = \gamma_{i,2}$ and $\eta_i = \eta_{i,1} = \eta_{i,2}$) corresponds to $\beta = A_1 = \delta_1 = \delta_2 = 1$ and $c_\star^2 = \gamma_i/\eta_i = \gamma_{i,1}/\eta_{i,1} = \gamma_{i,2}/\eta_{i,2}$.

The roots of the characteristic polynomial of Equation (39) are

$$w_{h,1}^2 = \frac{c_\star^2}{h^2}\left[\sigma_1(\omega) + \sigma_3(\omega) + \frac{\sigma_2(\omega)}{\sigma_3(\omega)}\right], \tag{45}$$

$$w_{h,2}^2 = \frac{c_\star^2}{h^2}\left[\sigma_1(\omega) - \frac{1}{2}\left(\sigma_3(\omega) + \frac{\sigma_2(\omega)}{\sigma_3(\omega)}\right) + \frac{\sqrt{3}}{2}\left(\sigma_3(\omega) - \frac{\sigma_2(\omega)}{\sigma_3(\omega)}\right)I\right], \tag{46}$$

$$w_{h,3}^2 = \frac{c_\star^2}{h^2}\left[\sigma_1(\omega) - \frac{1}{2}\left(\sigma_3(\omega) + \frac{\sigma_2(\omega)}{\sigma_3(\omega)}\right) - \frac{\sqrt{3}}{2}\left(\sigma_3(\omega) - \frac{\sigma_2(\omega)}{\sigma_3(\omega)}\right)I\right], \tag{47}$$

where

$$\sigma_1(\omega) = \frac{2}{3}(2\delta_1\omega^2 + 45A_1), \qquad \sigma_2(\omega) = \sigma_1^2(\omega) - 40(15\beta^2 - 2\delta_2\omega^2), \tag{48}$$

$$\sigma_3(\omega) = \left(\sqrt{\sigma^2(\omega) - \sigma_2^3(\omega)} + \sigma(\omega)\right)^{1/3}, \tag{49}$$

$$\sigma(\omega) = \frac{\sigma_1(\omega)}{2}\left(3\sigma_2(\omega) - \sigma_1^2(\omega)\right) + 3600\beta^2\omega^2. \tag{50}$$

As expected, the roots obtained here reduce to the homogeneous case considered in [1] when $\beta = A_1 = \delta_1 = \delta_2 = 1$.

The Taylor series expansions of σ_1, $\sigma_3 + \sigma_2/\sigma_3$ and $\sigma_3 - \sigma_2/\sigma_3$ up to second order are given by

$$\sigma_1 = 30A_1 + \mathcal{O}(k^2h^2), \tag{51}$$

$$\sigma_3 + \sigma_2/\sigma_3 = 3^{1/3}10\vartheta^{1/3} + 3^{2/3}10(3A_1^2 - 2\beta^2)\vartheta^{-1/3} + \mathcal{O}(k^2h^2), \tag{52}$$

$$\sigma_3 - \sigma_2/\sigma_3 = 3^{1/3}10\vartheta^{1/3} - 3^{2/3}10(3A_1^2 - 2\beta^2)\vartheta^{-1/3} + \mathcal{O}(k^2h^2), \tag{53}$$

where $\vartheta = 9A_1(A_1^2 - \beta^2) + \sqrt{3(9A_1^2 - 8\beta^2)}I$ and it is worth noting that ϑ is complex because $9A_1^2 - 8\beta^2 > 0$ (see Appendix A.2).

Using the polar representation of ϑ and the De Moivre's theorem [18], the Taylor series expansions of $\sigma_3 + \sigma_2/\sigma_3$ and $\sigma_3 - \sigma_2/\sigma_3$ can be written as

$$\sigma_3 + \sigma_2/\sigma_3 = 20\sqrt{3(3A_1^2 - 2\beta^2)}\cos(\theta/3) + \mathcal{O}(k^2h^2), \tag{54}$$

$$\sigma_3 - \sigma_2/\sigma_3 = 20\sqrt{3(3A_1^2 - 2\beta^2)}\sin(\theta/3)I + \mathcal{O}(k^2h^2), \tag{55}$$

where

$$\tan(\theta) = \frac{\sqrt{3(9A_1^2 - 8\beta^2)}}{9A_1(A_1^2 - \beta^2)}. \tag{56}$$

These expressions lead to the following Taylor expansions of the roots in Equations (45), (46) and (47)

$$w_{h,1}^2 = c_\star^2k^2\left[\frac{1}{h^2}\left(30A_1 + 20\sqrt{3(3A_1^2 - 2\beta^2)}\cos(\theta/3)\right) + \mathcal{O}(1)\right], \tag{57}$$

$$w_{h,2}^2 = c_\star^2k^2\left[\frac{1}{h^2}\left(30A_1 - 20\sqrt{3(3A_1^2 - 2\beta^2)}\cos((\theta+\pi)/3)\right) + \mathcal{O}(1)\right], \tag{58}$$

$$\begin{aligned} w_{h,3}^2 &= c_\star^2k^2\left[\frac{1}{h^2}\left(30A_1 - 20\sqrt{3(3A_1^2 - 2\beta^2)}\cos((\theta-\pi)/3)\right) + \mathcal{O}(1)\right] \\ &= c_\star^2k^2\left[1 + \mathcal{O}(k^2h^2)\right]. \end{aligned} \tag{59}$$

where it can be observed that Equation (59) corresponds to an approximation of the dispersion relation of the wave equation whereas Equations (57) and (58) correspond to two parasitic waves. As pointed out in Section 3.1, the objective of presenting the Taylor expansion of the roots is to distinguish the parasitic waves from the physical wave and not to analyse the accuracy of the roots as the element size h tends to zero.

To show that $30A_1 = 20\sqrt{3(3A_1^2 - 2\beta^2)}\cos((\theta - \pi)/3)$ (i.e. the root $w_{h,3}$ corresponds to the physical wave), the roots of the polynomial $S(x) = 4x^3 - 3x - \cos(\phi)$ are considered, namely $\cos(\phi/3)$, $\cos((2\pi + \phi)/3)$ and $\cos((4\pi + \phi)/3)$. As $x_\star = 3A_1(3A_1^2 - 2\beta^2)/(2|\vartheta|)$ is a root of $S(x)$ for $\phi = \theta - \pi$, it is clear that $x_\star$ must be equal to one of the three roots $x_1 = \cos((\theta - \pi)/3)$, $x_2 = \cos((\theta + \pi)/3)$ and $x_3 = \cos((\theta + 3\pi)/3)$. The polar decomposition of ϑ implies $0 \le \theta \le \pi$ because $\sin\theta = \Im\{\vartheta\}/|\vartheta| \ge 0$. Therefore $x_1 \in (1/2, 1)$, $x_2 \in (-1/2, 1/2)$ and $x_3 \in (-1, -1/2)$. Finally, the positivity of β implies that $30A_1/(20\sqrt{3(3A_1^2 - 2\beta^2)}) = 1/(2\sqrt{1 - 2\beta^2/(9A_1^2)}) \ge 1/2$ and therefore $x_\star = x_1$, which implies that the third root $w_{h,3}$ corresponds to the physical wave.

4.2. Stability for the Leap-Frog scheme

The dispersion relations for the SEM with a Leap-Frog time integrator are given by

$$\frac{4}{\Delta t^2}\sin^2\left(\frac{w_{h,l}^2 \Delta t}{2}\right) = w_{h,l}^2, \qquad \text{for } l = 1, 2, 3. \tag{60}$$

The stability of the discrete scheme is controlled by the conditions

$$\sqrt{\max_{l=1,2,3}\left\{\sup_{\omega\in[-1,1]} w_{h,l}^2(\omega), 0\right\}} \le \frac{2}{\Delta t}. \tag{61}$$

In this case, the maximum of the functions cannot be obtained explicitly so the strategy described in [1] is followed. Setting $kh = 2\pi K$ and $\lambda_l = h^2 w_{h,l}^2/c_\star^2$, for $l = 1, 2, 3$, and using that $w_{h,l}^2$ are the roots of the characteristic polynomial, leads to

$$P(\lambda_l) = \lambda_l^3 - 90A_1\lambda_l^2 + 1800\beta^2\lambda_l - 4\omega^2 T(\lambda_l) = 0. \tag{62}$$

with $\omega = \sin(\pi K)$ and $T(\lambda_l) = \delta_1\lambda_l^2 + 60\delta_2\lambda_l + 1800\beta^2$.

Taking the derivative of Equation (62) with respect to K and noting that the maximum of λ_l, and consequently the maximum of $w_{h,l}^2$, is attained when $d\lambda_l/dK = 0$, leads to

$$\omega\sqrt{1-\omega^2}T(\lambda_l) = 0. \tag{63}$$

Equation (63) contains three classes of solutions. As discussed in Appendix A, the only two solutions relevant from the point of view of the stability of the Leap-Frog scheme are

$$\chi_2 = 15\left(3A_1 + \sqrt{9A_1^2 - 8\beta^2}\right), \qquad \chi_4 = \left[\tau_1 + \tau_3 + \frac{\tau_2}{\tau_3}\right], \tag{64}$$

where $\tau_i = \sigma_i(1)$ for $i = 1, 2, 3$.

The stability condition is therefore given by

$$\alpha = \frac{c_\star \Delta t}{h} \leq \alpha_M, \tag{65}$$

with

$$\alpha_M = \frac{2}{\max\{\sqrt{\chi_2}, \sqrt{\chi_4}\}}. \tag{66}$$

It is worth noting that for a homogeneous medium the polynomial T, which reduces to the case presented in [1], has no real roots and there are only two classes of solutions. It can also be observed that the well known homogeneous stability condition $\alpha_M = 2/\sqrt{6(7+\sqrt{29})} \approx 0.23$ (see Table 1) is recovered when $\beta = A_1 = \delta_1 = \delta_2 = 1$.

4.3. Numerical examples

Three numerical examples are considered to validate the stability condition derived in this Section and to illustrate that using a condition derived for the homogeneous case can lead to either unstable results or inefficient simulations. The domain $\Omega = [0, 1]$ is considered and the material parameters are defined as

$$\gamma(x) = \phi_1 + \phi_2 \sin(2\pi x/h + \phi_3), \qquad \eta(x) = \psi_1 + \psi_2 \sin(2\pi x/h + \psi_3) \tag{67}$$

where the constants ϕ_i and ψ_i, for $i = 1, 2, 3$ are selected so that $\gamma(x_i) = \gamma_i$, $\gamma(x_{i,1}) = \gamma_{i,1}$, $\gamma(x_{i,2}) = \gamma_{i,2}$, $\eta(x_i) = \eta_i$, $\eta(x_{i,1}) = \eta_{i,1}$ and $\eta(x_{i,2}) = \eta_{i,2}$.

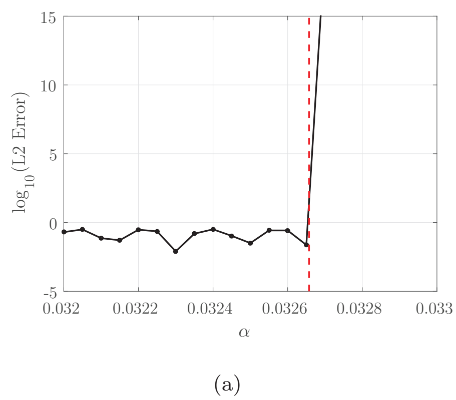

Figure 4: Relative error in the $\mathcal{L}^2(\Omega)$ norm as a function of $\alpha = c_\star \Delta t/h$ for (a) $Q_{\gamma,1} = Q_{\gamma,2} = 10$, $Q_{\eta,1} = Q_{\eta,2} = 1/10$ and (b) $Q_{\gamma,1} = 1$, $Q_{\gamma,2} = 1/10$, $Q_{\eta,1} = Q_{\eta,2} = 1/10$. The discontinuous line represents the stability limit corresponding to α_M.

The analytical solution given in Equation (38) is again considered and the initial, boundary conditions and source term are derived from the exact solution as usually done in the method of manufactured solutions. In all the examples, the solution is advanced in time up to a final time $T = 10$ and the relative error in the $\mathcal{L}^2(\Omega)$ norm is measured. Analogously to the previous examples in Section 3.4, the goal is to evaluate the accuracy of the stability limit derived for cubic spectral elements with a periodic fluctuation of the material properties and not to study the accuracy of the numerical scheme.

The first example considers $\gamma_i = 10$, $\gamma_{i,1} = 1$, $\gamma_{i,2} = 1$, $\eta_i = 1$, $\eta_{i,1} = 10$ and $\eta_{i,2} = 10$. The stability condition from Equation (66) is $\alpha_M \approx 0.03265$ and it is given by the first term in the maximum in Equation (66). Figure 4 (a) shows the relative error in the $\mathcal{L}^2(\Omega)$ norm as a function of the value of α considered to define the time step Δt for a uniform mesh with $h = 0.01$. It can be clearly observed that when the time step is defined by using a value of $\alpha \leq \alpha_M$ stability is guaranteed, whereas a value of $\alpha > \alpha_M$ leads to unstable results. In this example, if the time step is computed using the results derived from the homogeneous case, as detailed in Equation (36), the time step would be selected as $\Delta t \approx 2.15 \times 10^{-3}$ clearly leading to unstable results as it is more

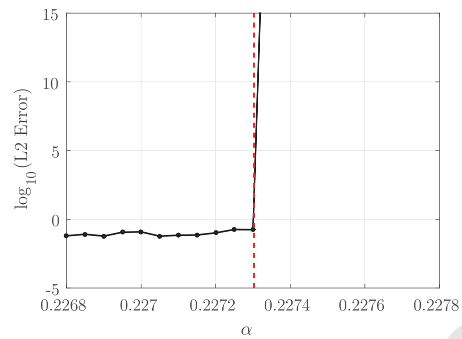

Figure 5: Relative error in the $\mathcal{L}^2(\Omega)$ norm as a function of $\alpha = c_\star \Delta t/h$ for $\gamma_i = 1$, $\gamma_{i,1} = 1$, $\gamma_{i,2} = 10$, $\eta_i = 10$, $\eta_{i,1} = 10$ and $\eta_{i,2} = 1$. The discontinuous line represents the stability limit corresponding to α_M.

than two times higher than the bound derived for the heterogeneous case, i.e. $\Delta t \leq 8.78 \times 10^{-4}$.

The second example considers $\gamma_i = 1$, $\gamma_{i,1} = 1$, $\gamma_{i,2} = 10$, $\eta_i = 1$, $\eta_{i,1} = 10$ and $\eta_{i,2} = 10$. The stability condition from Equation (66) is $\alpha_M \approx 0.073814$ and it is now given by the second term in the maximum in Equation (66). Figure 4 (b) shows the relative error in the $\mathcal{L}^2(\Omega)$ norm as a function of the value of α considered to define the time step Δt for a uniform mesh with $h = 0.01$. Again, the results illustrate the validity of the stability limit found in this Section. In this example, if the time step is computed using the results derived from the homogeneous case ($\Delta t \approx 6.81 \times 10^{-3}$) unstable results are obtained as the stability limit induces a time step more than four times smaller, i.e. $\Delta t \leq 1.55 \times 10^{-3}$.

The last example considers a case where the time step computed using the homogeneous results leads to stable results but the simulation is less efficient than if the time step was computed from the heterogeneous bound presented in this Section. The material parameters are given by $\gamma_i = 1$, $\gamma_{i,1} = 1$, $\gamma_{i,2} = 10$, $\eta_i = 10$, $\eta_{i,1} = 10$ and $\eta_{i,2} = 1$. Figure 5 shows the relative error in the $\mathcal{L}^2(\Omega)$ norm as a function of the value of α considered to define the time step Δt for a uniform mesh with $h = 0.01$. Once more, the validity of the proposed stability limit is clearly demonstrated. In this case both terms in the maximum in Equation (66) have a similar value, namely $\chi_2 \approx 77.41$ and $\chi_4 \approx 75.19$. If the time step is computed using the results derived from the homogeneous case, the time step would be selected as $\Delta t \approx 2.15 \times 10^{-3}$, exactly the same as in the first example, leading to stable results here. When compared to the stability limit for the heterogenerous case (i.e. $\Delta t \approx 4.08 \times 10^{-3}$), the results reveal that the simulation using the time step computed from the homogeneous case results in almost twice the cost of the simulation with the time step computed from the heterogeneous stability limit.

5. Extensions

This Section briefly discusses three extensions of the analysis presented in detail for quadratic and cubic spectral elements in Sections 3 and 4 respectively. The extension to high-order polynomial approximations, larger periodicity of the material parameter fields and higher dimensions are considered.

5.1. Higher order polynomial approximations

The Von Neumann stability analysis described in previous sections can be extended to any order of the polynomial approximation. A detailed analysis, as presented for the quadratic and cubic case, is difficult due to the increase of the degree of the characteristic polynomial with the order of the polynomial approximation. However, with the aid of a symbolic package it is possible to obtain an exact expressions of the stability limit for a degree of approximation $p = 4$. For higher orders, it is always possible to obtain an accurate approximation of the stability limit by employing standard root finding algorithms (e.g. Newton-Raphson) to estimate the value of the roots of the characteristic polynomial.

Two examples are considered to validate the stability condition derived for $p = 4$. The domain $\Omega = [0, 1]$ is considered and the material parameters are

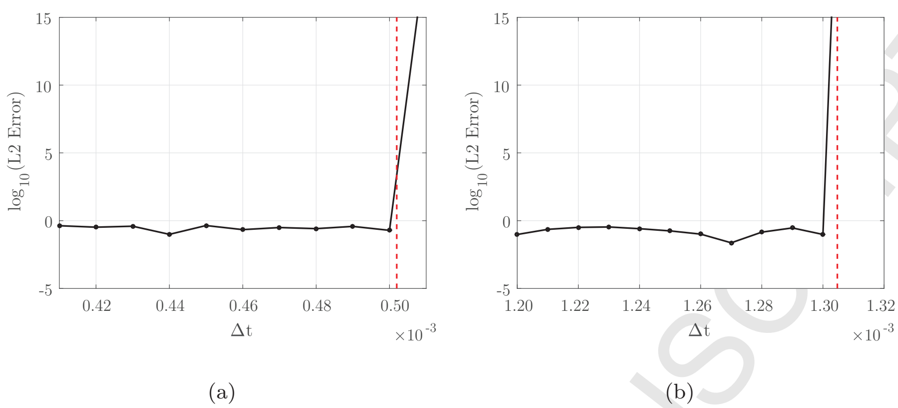

Figure 6: Relative error in the $\mathcal{L}^2(\Omega)$ norm as a function of Δt for (a) $\gamma_i = 10$, $\gamma_{i,1} = 1$, $\gamma_{i,2} = 1$, $\gamma_{i,3} = 10$, $\eta_i = 1$, $\eta_{i,1} = 10$, $\eta_{i,2} = 10$, $\eta_{i,1} = 1$ and (b) $\gamma_i = 4$, $\gamma_{i,1} = 2$, $\gamma_{i,2} = 1$, $\gamma_{i,3} = 5$, $\eta_i = 3$, $\eta_{i,1} = 6$, $\eta_{i,2} = 1$, $\eta_{i,1} = 4$. The discontinuous line represents the stability limit.

defined as

$$\gamma(x) = \phi_1 + \phi_2 \sin(2\pi x/h) + \phi_3 \cos(2\pi x/h) + \phi_4 \sin^2(2\pi x/h)\,, \tag{68a}$$

$$\eta(x) = \psi_1 + \psi_2 \sin(2\pi x/h) + \psi_3 \cos(2\pi x/h) + \psi_4 \sin^2(2\pi x/h) \tag{68b}$$

where the constants ϕ_i and ψ_i, for $i = 1, \ldots, 4$, are selected so that $\gamma(x_i) = \gamma_i$, $\gamma(x_{i,k}) = \gamma_{i,k}$, $\eta(x_i) = \eta_i$ and $\eta(x_{i,k}) = \eta_{i,k}$ for $k = 1 \ldots, 3$. The analytical solution given in Equation (38) is again considered.

The first example considers $\gamma_i = 10$, $\gamma_{i,1} = 1$, $\gamma_{i,2} = 1$, $\gamma_{i,3} = 10$, $\eta_i = 1$, $\eta_{i,1} = 10$, $\eta_{i,2} = 10$ and $\eta_{i,1} = 1$. The stability condition derived with the aid of a symbolic package is $\Delta t \approx 5.0197 \times 10^{-3}$. Figure 6 (a) shows the relative error in the $\mathcal{L}^2(\Omega)$ norm as a function of the time step Δt for a uniform mesh with $h = 0.01$. A second example is considered with $\gamma_i = 4$, $\gamma_{i,1} = 2$, $\gamma_{i,2} = 1$, $\gamma_{i,3} = 5$, $\eta_i = 3$, $\eta_{i,1} = 6$, $\eta_{i,2} = 1$ and $\eta_{i,1} = 4$. The stability condition is $\Delta t \approx 1.3047 \times 10^{-3}$. Figure 6 (b) shows the relative error in the $\mathcal{L}^2(\Omega)$ norm as a function of the time step Δt.

In both cases, the results demonstrate the validity of the stability limit obtained for quartic spectral elements.

5.2. Larger periodicity of the material parameter fields

The extension to problems involving material properties whose periodicity is larger than a single element is also possible using the Von Neumann analysis described in previous sections. Once more, the difficulty increases due to the higher degree of the characteristic polynomial. With the aid of a symbolic package, it is possible to obtain an exact expressions of the stability limit only for quadratic spectral elements and periodicity equals to $2h$, where h is the characteristic element size. For higher orders approximations with periodicity $2h$ or for larger periodicities, it is always possible to obtain an accurate approximation of the stability limit by employing standard root finding algorithms.

Two examples are considered to validate the stability condition derived for quadratic spectral elements and periodicity $2h$. The domain $\Omega = [0, 1]$ is considered and the material parameters are defined in Equation (68). In this case, the constants ϕ_i and ψ_i, for $i = 1, \ldots, 4$, are selected so that $\gamma(x_1^{2k+1}) = \gamma_1^{2k+1}$, $\gamma(x_{i,1}^{2k+1}) = \gamma_{i,1}^{2k+1}$, $\gamma(x_1^{2k}) = \gamma_1^{2k}$, $\gamma(x_{i,1}^{2k}) = \gamma_{i,1}^{2k}$, $\eta(x_1^{2k+1}) = \eta_1^{2k+1}$, $\eta(x_{i,1}^{2k+1}) = \eta_{i,1}^{2k+1}$, $\eta(x_1^{2k}) = \eta_1^{2k}$ and $\eta(x_{i,1}^{2k}) = \eta_{i,1}^{2k}$ where the superscript is used to specify odd and even element numbers.

The first example considers $\gamma_1^{2k+1} = 10$, $\gamma_{i,1}^{2k+1} = 1$, $\gamma_1^{2k} = 1$, $\gamma_{i,1}^{2k} = 10$, $\eta_1^{2k+1} = 1$, $\eta_{i,1}^{2k+1} = 10$, $\eta_1^{2k} = 10$ and $\eta_{i,1}^{2k} = 1$. The stability condition derived with the aid of a symbolic package is $\Delta t \approx 1.7167 \times 10^{-3}$. Figure 7 (a) shows the relative error in the $\mathcal{L}^2(\Omega)$ norm as a function of the time step Δt for a uniform mesh with $h = 0.01$. A second example is considered with $\gamma_1^{2k+1} = 4$, $\gamma_{i,1}^{2k+1} = 2$, $\gamma_1^{2k} = 1$, $\gamma_{i,1}^{2k} = 5$, $\eta_1^{2k+1} = 3$, $\eta_{i,1}^{2k+1} = 6$, $\eta_1^{2k} = 1$ and $\eta_{i,1}^{2k} = 4$. The stability condition is $\Delta t \approx 3.6820 \times 10^{-3}$. Figure 7 (b) shows the relative error in the $\mathcal{L}^2(\Omega)$ norm as a function of the time step Δt.

The results demonstrate the validity of the stability limit obtained for a larger periodicity of the material parameter fields with quadratic approximation. It is also worth noting that the magnitude of the material parameters at the mesh nodes is the same as in the example with $p = 4$ spectral elements. However, it is clear from the numerical results in Figures 6 and 7 that the stability limit is significantly different, being more restrictive for high order approximations.

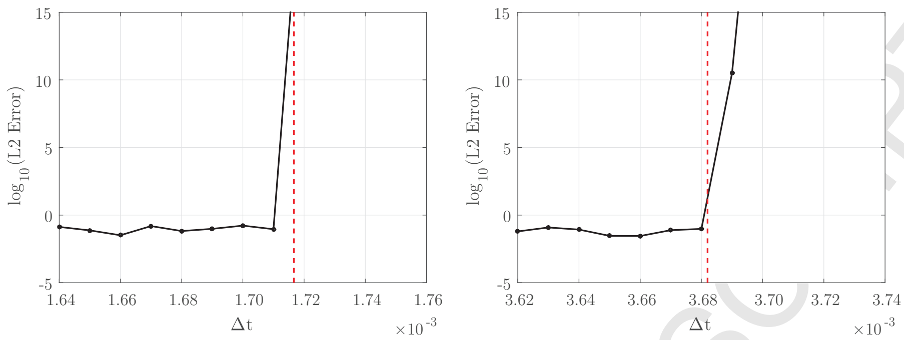

(a) (b)

Figure 7: Relative error in the $\mathcal{L}^2(\Omega)$ norm as a function of Δt for (a) $\gamma_1^{2k+1} = 10$, $\gamma_{i,1}^{2k+1} = 1$, $\gamma_1^{2k} = 1$, $\gamma_{i,1}^{2k} = 10$, $\eta_1^{2k+1} = 1$, $\eta_{i,1}^{2k+1} = 10$, $\eta_1^{2k} = 10$, $\eta_{i,1}^{2k} = 1$ and (b) $\gamma_1^{2k+1} = 4$, $\gamma_{i,1}^{2k+1} = 2$, $\gamma_1^{2k} = 1$, $\gamma_{i,1}^{2k} = 5$, $\eta_1^{2k+1} = 3$, $\eta_{i,1}^{2k+1} = 6$, $\eta_1^{2k} = 1$, $\eta_{i,1}^{2k} = 4$. The discontinuous line represents the stability limit.

5.3. Higher dimensions

Following the methodology described in [1, Section 12.2] (and originally derived in [19, 20]) for homogeneous materials, the results presented in this paper for one-dimensional problems can be easily extended to higher dimensions when the functions that describe the material properties can be written as a tensor product of one-dimensional functions.

Assuming the following decomposition in d dimensions:

$$\eta(x_1, \ldots, x_d) = \prod_{k=1}^{d} \eta^k(x_k) \qquad \gamma(x_1, \ldots, x_d) = \prod_{k=1}^{d} \gamma^k(x_k), \tag{69}$$

where $\eta^k(x_k)$ and $\gamma^k(x_k)$ denote the one-dimensional material field in the x_k direction, it can be shown, using an extension of the original method described in previous sections, that the roots of the characteristic equation correspond to the sum of the roots of the one-dimensional characteristic equations corresponding to one-dimensional material fields

$$w_{h,l_d}^2(\omega) = \sum_{k=1}^{d} w_{h,l,k}^2(\omega), \qquad l = 1, \ldots, p, \quad k = 1, \ldots, d \tag{70}$$

where $w_{h,l,k}(\omega)$ denotes a root of Equation (21) with parameter fields $\eta^k(x_k)$ and $\gamma^k(x_k)$. The stability limit can be written as

$$\Delta t \leq \frac{2}{\sqrt{\max\limits_{1\leq l\leq p}\left\{\sup\limits_{\omega\in[-1,1]}\left(\sum_{k=1}^{d} w_{h,l,k}^2(\omega)\right), 0\right\}}}. \tag{71}$$

With the aid of a symbolic package, it is possible to find the supremum of Equation (71) for quadratic elements in two dimensions. For higher orders in two dimensions, or higher dimensions, the supremum can be found by using standard root finding algorithms.

Alternatively, an upper bound of the roots of the characteristic polynomial corresponding to the multi-dimensional problem can be expressed as

$$\max_{1\leq l\leq p}\left\{\sup_{\omega\in[-1,1]}\left(\sum_{k=1}^{d} w_{h,l,k}^2(\omega)\right), 0\right\} \leq \sum_{k=1}^{d}\left(\max_{1\leq l\leq p}\left\{\sup_{\omega\in[-1,1]} w_{h,l,k}^2(\omega), 0\right\}\right) \tag{72}$$

and a conservative stability limit, using results from the one-dimensional analysis, reads

$$\Delta t \leq \frac{2}{\sqrt{\sum\limits_{k=1}^{d}\left(\max\limits_{1\leq l\leq p}\left\{\sup\limits_{\omega\in[-1,1]} w_{h,l,k}^2(\omega), 0\right\}\right)}}. \tag{73}$$

It is worth noting that, if Equation (72) is an equality, then the stability limit derived from a one-dimensional analysis is exact. Furthermore, when $w_{h,l,1} = \ldots = w_{h,l,d}$, for $l = 1, \ldots, p$, the stability limit in d dimensions is obtained by dividing the one-dimensional stability limit by $\sqrt{d}$. A particular case corresponds to a medium where the material properties in each dimension coincide, that is $\eta^1(x_1) = \ldots = \eta^d(x_d)$ and $\gamma^1(x_1) = \ldots = \gamma^d(x_d)$. This confirms the results detailed in [1] for a homogeneous medium.

In the case of non-tensorised material properties (i.e. when Equation (69) is not verified), one-dimensional results cannot be employed and the Von Neumann stability analysis must be repeated for the full multi-dimensional problem.

Two examples in two dimensions are considered to validate the stability limits derived for the multi-dimensional case with quadratic spectral elements.

The domain $\Omega = [0,1]^2$ is considered and the material parameters are defined, similarly to the one-dimensional case with $p = 2$ presented in Section 3, as

$$\gamma^1(x) = \gamma_i^1 + (\gamma_{i,1}^1 - \gamma_i^1)\sin^2(\pi x/h), \qquad \eta^1(x) = \eta_i^1 + (\eta_{i,1}^1 - \eta_i^1)\sin^2(\pi x/h), \tag{74a}$$

$$\gamma^2(x) = \gamma_i^2 + (\gamma_{i,1}^2 - \gamma_i^2)\sin^2(\pi x/h), \qquad \eta^2(x) = \eta_i^1 + (\eta_{i,1}^2 - \eta_i^2)\sin^2(\pi x/h). \tag{74b}$$

The first example considers a material with $\gamma_i^1 = 1$, $\gamma_{i,1}^1 = 3$, $\gamma_i^2 = 2$, $\gamma_{i,1}^2 = 4$, $\eta_i^1 = 2$, $\eta_{i,1}^1 = 6$, $\eta_i^2 = 4$ and $\eta_{i,1}^2 = 8$. Figure 8 (a) shows the $\mathcal{L}^2(\Omega)$ norm of the solution at time $T = 10$ as a function of Δt. The red and blue discontinuous lines represent the stability limit of Equations (71) and (73) respectively. It can be clearly observed that the stability limit derived for the multi-dimensional problem is exact whereas the stability limit derived from the one-dimensional analysis is conservative due to the bound introduced in Equation (72). A second example is considered using a medium that leads to an equality in Equation (72), meaning that the stability limit in Equation (73) is exact. Figure 8 (b) shows the $\mathcal{L}^2(\Omega)$ norm of the solution at time $T = 10$ as a function of Δt for a material with $\gamma_i^1 = 1$, $\gamma_{i,1}^1 = 3$, $\gamma_i^2 = 1$, $\gamma_{i,1}^2 = 3$, $\eta_i^1 = 2$, $\eta_{i,1}^1 = 6$, $\eta_i^2 = 2$ and $\eta_{i,1}^2 = 6$. In this case the red and blue lines are overlapped as the two stability limits given by Equations (71) and (73) coincide.

6. Numerical examples in randomly fluctuating media

This Section presents a number of examples of wave propagation in randomly heterogeneous media. The periodicity hypothesis for the material properties does not hold and therefore, the stability analyses in Sections 3 and 4 are theoretically not valid. However, the objective is to show that the criteria developed in this paper still provide reasonable estimates for the stability in more complex scenarios.

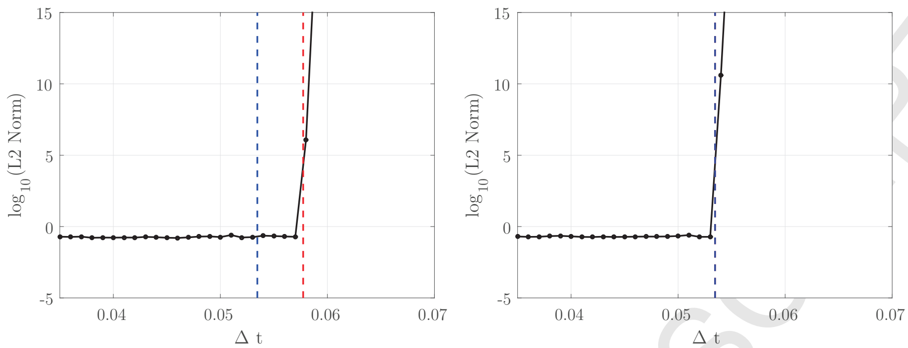

(a) (b)

Figure 8: $\mathcal{L}^2(\Omega)$ norm of the solution at time $T = 10$ as a function of Δt for (a) $\gamma_i^1 = 1$, $\gamma_{i,1}^1 = 3$, $\gamma_i^2 = 2$, $\gamma_{i,1}^2 = 4$, $\eta_i^1 = 2$, $\eta_{i,1}^1 = 6$, $\eta_i^2 = 4$, $\eta_{i,1}^2 = 8$ and (b) $\gamma_i^1 = 1$, $\gamma_{i,1}^1 = 3$, $\gamma_i^2 = 1$, $\gamma_{i,1}^2 = 3$, $\eta_i^1 = 2$, $\eta_{i,1}^1 = 6$, $\eta_i^2 = 2$, $\eta_{i,1}^2 = 6$. The red and blue discontinuous lines represent the stability limit of Equations (71) and (73) respectively. In (b), the red and blue lines overlap.

6.1. Stability of wave propagation in quasi-periodic randomly heterogeneous media

The propagation of a wave in $\Omega = [0, 1]$ is considered. The domain is meshed with 20 elements of length $h = 0.05$. The material properties are randomly fluctuating within the elements, but always take the same value at the vertices (see two examples in Figure 9). More specifically, the parameters at all the vertices are $\eta_i = 5$ and $\gamma_i = 2$, whereas within the elements (one node for quadratic polynomials, and two nodes for cubic polynomials) they are realisations of independent log-normal random variables with averages $\underline{\eta} = \mathbb{E}[\eta(x)] = 5$ and $\underline{\gamma} = \mathbb{E}[\gamma(x)] = 2$ and variances $\sigma_\eta^2 = \mathbb{E}[(\eta(x) - \underline{\eta})^2] = 32$ and $\sigma_\gamma^2 = \mathbb{E}[(\gamma(x) - \underline{\gamma})^2] = 2$. Although there is no analytical solution for this problem, the same boundary conditions, initial conditions and source term as in the examples of Section 3.4 are considered. In all the examples, the solution is advanced in time up to a final time $T = 10$ and the $\mathcal{L}^2(\Omega)$ norm of the solution $u(x, T)$ is measured.

The stability limits of Equation (32) and (66) are modified slightly because the equivalent velocity $c_\star$ is not constant throughout the elements. The stability

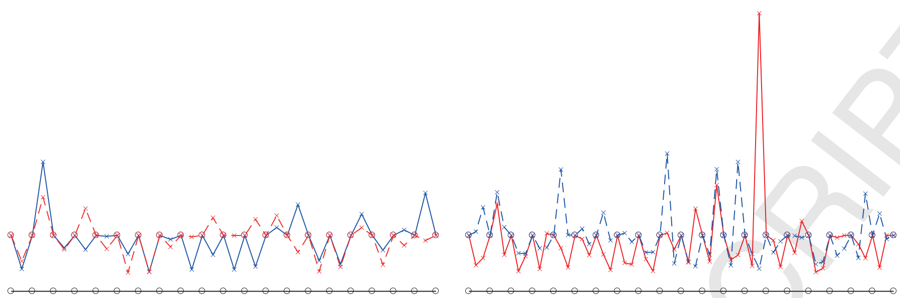

(a) (b)

Figure 9: Two realisations of the quasi-periodic randomly fluctuating properties for (a) quadratic and (b) cubic polynomials. The solid and dashed fluctuating lines represent the two realisations, respectively, and the lower line represents the mesh elements. The circles indicate the position of the vertices.

limit is therefore taken directly in terms of the time step as

$$\Delta t \leq h \min\left(\frac{\alpha_M}{c_\star}\right), \tag{75}$$

365 where the minimum is taken over all elements of the mesh, and α_M is given by Equation (32) with element-dependent β and δ, and (66) with element-dependent β, δ_1, δ_2 and A_1, for quadratic and cubic polynomials, respectively. As only 20 elements are considered, there is a strong variability of the time step (and the actual stability limit) computed for different realisations of the material properties. Figure 10 presents the probability density function (PDF) of the time step Δt computed with Equation (75) for different realisations of the 20 elements-long bar. As this PDF depends on the length, three different lengths are considered. The estimations of the PDFs are obtained through Monte Carlo sampling with 100,000 realisations and 50 bins for the histogram. As expected, it can be observed that the stability limit becomes more stringent for longer domains, for both quadratic and cubic polynomials. It is also interesting to note that the heterogeneous stability limit is systematically higher than the homogeneous stability limit (for this particular setting), which means that using the homogeneous criterion would yield an unnecessary higher computational cost.

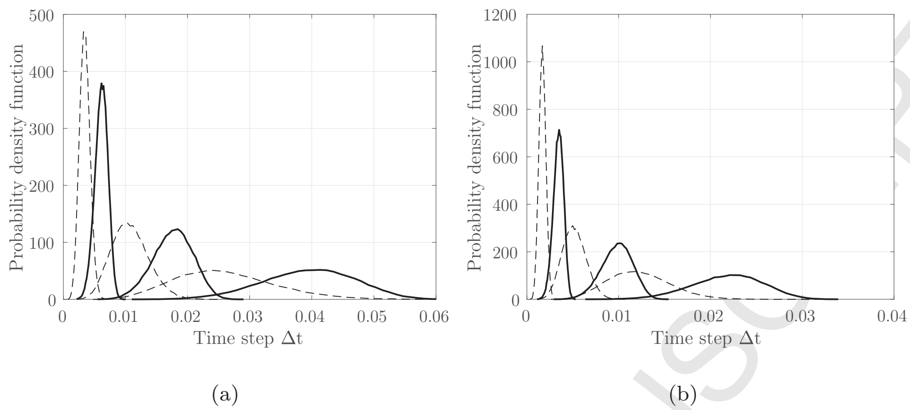

Figure 10: Probability density function of the time step Δt computed with Equation (75) for (a) quadratic and (b) cubic polynomials. The three solid lines correspond to lengths of 10, 20 and 50 elements respectively (the smallest Δt corresponds to the longest domain) and the thin dashed line corresponds to the homogeneous stability criterion of Equation (36) for the same lengths.

Figure 11 presents stability results, obtained for three different realisations of the 20-element domain described above. As expected, the stability criterion is not as precise as in the periodic case, since the theoretical derivation is not applicable, but it is interesting to note that, for the three realisations considered, the stability constant is both conservative and accurate. It is conservative in the sense that instability seems to arise for larger time steps than predicted by the stability coefficient. It is accurate in the sense that there is a very small difference between the time step predicted and the time step for which instability arises. This stability limit is compared to the homogeneous stability criterion of Equation (36), which confirms the previous observation that the homogeneous criterion is systematically overly conservative for this particular setting.

Finally, the relative distance to instability provided by the stability limit in Equation (75) is computed for 1,000 samples of 20 elements of the bar of the PDF. This relative distance is defined as

$$DtI = 2\frac{\Delta t_{\text{instab}} - \Delta t}{\Delta t_{\text{instab}} + \Delta t}, \tag{76}$$

where Δt_{instab} is the time step at which instability emerges for a given sample.

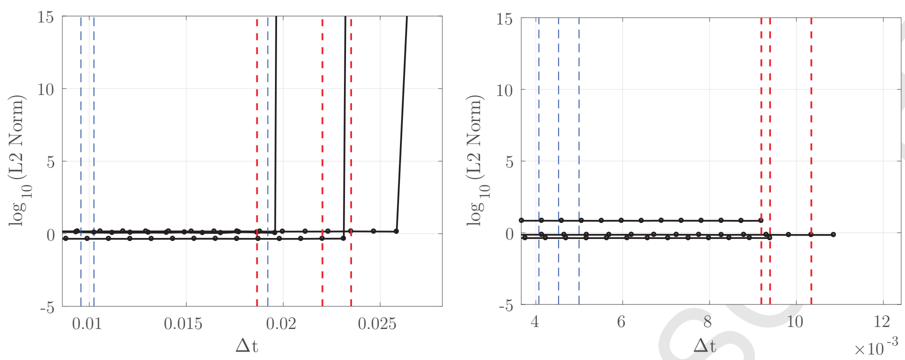

(a) (b)

Figure 11: $\mathcal{L}^2(\Omega)$ norm of the solution at time $T = 10$ as a function of Δt for three realisations of a quasi-periodic randomly fluctuating case with (a) quadratic and (b) cubic polynomials. The discontinuous red line represents the heterogeneous stability criterion of Equation (75), and the discontinuous blue line correspond to the homogeneous stability criterion of Equation (36).

This coefficient is clearly expected to be small if the stability limit is accurate and it is expected to be positive if the stability limit is conservative. The PDF for the relative distance to instability is approximated using 50 bins and represented in Figure 12. It is remarkable that, even though the theory is not directly applicable because the material properties are not periodic, the stability criterion is still both accurate and conservative. In particular, it is much more accurate than the homogeneous stability limit estimated with Equation (36). It is interesting to note that, even though it is mostly conservative, the homogeneous limit does induce instability in some cases (i.e. the dashed curve does not vanish completely for negative values of the instability limit in Figure 12), at least in the quadratic case.

6.2. Stability of wave propagation in randomly heterogeneous media

The following set of numerical examples considers the wave propagation in a randomly heterogeneous medium. The constraint of having the same value of the material properties in the mesh vertices is removed (see two examples

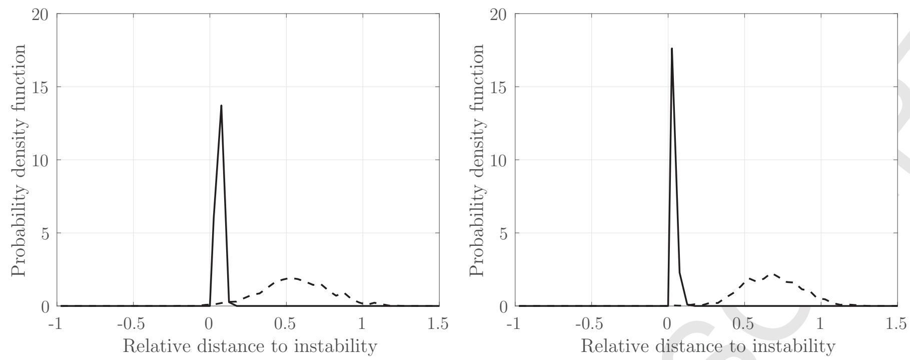

Figure 12: Probability density function of the relative distance (in time) to instability for quadratic (left figure) and cubic polynomials (right figure). The solid lines represent the heterogeneous stability criterion of Equation (75), and the discontinuous lines correspond to the homogeneous stability criterion of Equation (36).

in Figure 13) and the applicability of the stability limits derived for periodic material properties is studied numerically.

The parameters are realisations of statistically homogeneous random fields with log-normal first-order marginal densities with averages $\underline{\eta} = \mathbb{E}[\eta(x)] = 5$ and $\underline{\gamma} = \mathbb{E}[\gamma(x)] = 2$ and variances $\sigma_\eta^2 = \mathbb{E}[(\eta(x) - \underline{\eta})^2] = 32$ and $\sigma_\gamma^2 = \mathbb{E}[(\gamma(x) - \underline{\gamma})^2] = 2$. As in the previous examples, the random fields of the two parameters are assumed independent. The solution is advanced in time up to a final time $T = 10$ and the $\mathcal{L}^2(\Omega)$ norm of the solution $u(T)$ is measured.

Computing the solution for 1000 realisations of the random fields, either with quadratic or cubic polynomials, it is possible to construct the PDF of the relative distance to instability, as in Equation (76). These PDF are represented in Figure 14. Contrary to the case of the quasi-periodic fields, the heterogeneous stability criterion of Equation (75) is not always conservative, although it remains rather accurate. Comparing this limit to the homogeneous stability criterion of Equation (36), it is not very clear which estimate is the most appropriate for a given simulation. Indeed, in most cases, conservatism would probably be preferred over precision. Indeed, running into instability forces the user to restart the simulation completely, while a slightly over-constrained time

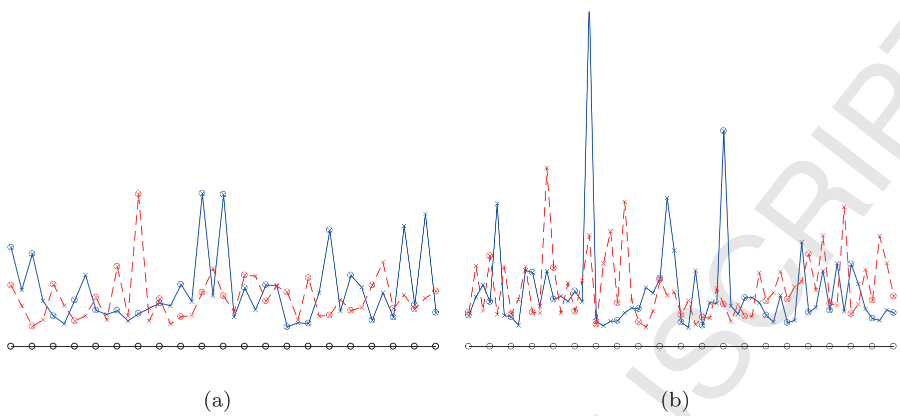

Figure 13: Two realisations of the non-periodic randomly-fluctuating properties for (a) quadratic and (b) cubic polynomials. The solid and dashed fluctuating lines represent the two realisations, respectively, and the lower line represents the mesh elements. The circles indicate the position of the vertices.

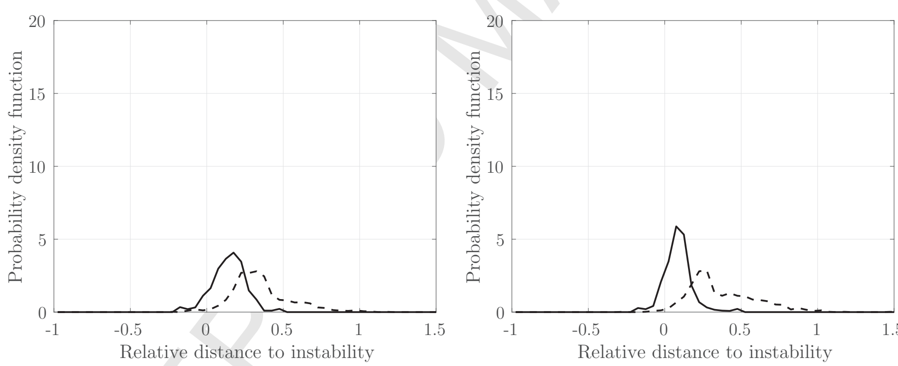

Figure 14: Probability density function of the relative distance (in time) to instability for quadratic (left figure) and cubic polynomials (right figure). The solid lines represent the heterogeneous stability criterion of Equation (75), and the discontinuous lines correspond to the homogeneous stability criterion of Equation (36).

step only means a longer simulation time. This conclusion remains the same for both quadratic and cubic polynomials.

6.3. Influence of correlation length

Finally, correlated random fields for the parameters are considered, instead of the white noise that was considered in previous examples with randomly fluctuating material properties. The first-order marginal densities of the random fields are the same as in the previous section. In addition, triangular power density spectra is considered, with correlation length $\ell_c = h$ and $\ell_c = 3h$. From these random models, realisations can be drawn (using for instance the spectral representation method [21]) to obtain values of the material parameters at the vertices and at the interior nodes. Computing the solution for 1,000 realisations of the random fields, either with quadratic or cubic polynomials, the PDFs of the relative distance to instability, as in Equation (76), are displayed in Figure 15. To better analyse the results, the results reported in Figure 14, which formally corresponds to $\ell_c = 0$, should be also considered. Similarly to the examples with randomly fluctuating material properties, the heterogeneous criterion is overall less conservative and more precise than the homogeneous criterion. As expected, the two curves are closer when the correlation length increases, since this corresponds to material properties being close to a homogeneous medium.

7. Concluding remarks

The stability of an explicit time marching algorithm for the spectral element method in a medium with periodically fluctuating material parameters has been discussed. A detailed Von Neumann stability analysis is presented for quadratic and cubic polynomial approximations under the assumption of periodic heterogeneous media with period equal to the characteristic element size. The theoretical stability limits are demonstrated to be valid using numerical examples. More important, the analysis reveals the origin of instabilities that are often observed when the stability limit derived for homogeneous materials is adapted by simply changing the velocity of the wave to account for the material heterogeneity. The numerical examples show that adapting homogeneous

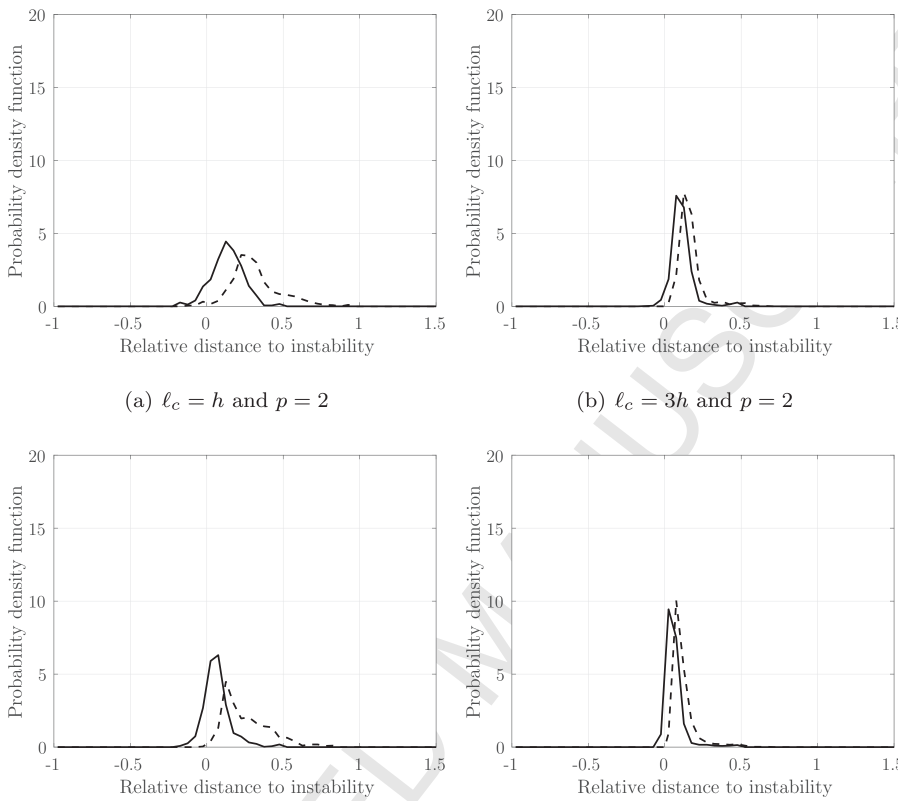

(a) $\ell_c = h$ and $p = 2$ (b) $\ell_c = 3h$ and $p = 2$

(c) $\ell_c = h$ and $p = 3$ (d) $\ell_c = 3h$ and $p = 3$

Figure 15: Probability density function of the relative distance (in time) to instability for 1000 realisations of correlated samples. The solid lines represent the heterogeneous stability criterion of Equation (75) and the discontinuous lines correspond to the homogeneous stability criterion of Equation (36).

formulae for heterogeneous media leads to either instability or to unnecessary increased computational resources.

Extensions of the results derived for quadratic and cubic one-dimensional spectral elements are discussed, including higher order approximations, different periodicity of the material parameters and higher dimensions. The main limitation of the analysis presented here is that exact formulas can only be derived when the degree of the characteristic polynomial is low (i.e. moderate polynomial orders of approximation, moderate period of the material parameters compared to the element sizes), despite the methodology is still applicable when combined with a root finding algorithm.

Extensive numerical results demonstrate the validity of the new stability limits derived for heterogeneous materials with periodic fluctuation. In addition, further numerical experiments of the stability for randomly fluctuating material properties are presented. These numerical experiments reveal that the stability limits derived for periodically fluctuating material properties are precise when the material parameters take the same value at the vertices of the mesh. In contrast, for fully randomly fluctuating material properties its accuracy is lower.

Acknowledgements

The authors would like to acknowledge the support provided by CentraleSupélec and the Erasmus+ programme for an invitation of the first author to CentraleSupélec and the second author to Swansea University respectively. The first author also gratefully acknowledges the financial support provided by the Sêr Cymru National Research Network for Advanced Engineering and Materials, United Kingdom.

References

[1] G. Cohen, Higher-order numerical methods for transient wave equations, Scientific Computation, Springer, 2001.

[2] J. D. De Basabe, M. K. Sen, Grid dispersion and stability criteria of some common finite-element methods for acoustic and elastic wave equations, Geophysics 72 (6) (2007) T81–T95.

[3] J. D. De Basabe, M. K. Sen, Stability of the high-order finite elements for acoustic or elastic wave propagation with high-order time stepping, Geophysical Journal International 181 (2010) 577–590.

[4] C. Agut, J. Diaz, Stability analysis of the interior penalty discontinuous Galerkin method for the wave equation, ESAIM: Mathematical Modelling and Numerical Analysis 47 (3) (2013) 903–932.

[5] W. Mulder, E. Zhebel, S. Minisini, Time-stepping stability of continuous and discontinuous finite-element methods for 3-d wave propagation, Geophysical Journal International 196 (2) (2014) 1123–1133.

[6] Y. Maday, E. M. Ronquist, Optimal error analysis of spectral methods with emphasis on non-constant coefficients and deformed geometries, ICASE Report 89-56, NASA Langley Research Center (1989).

[7] G. Seriani, E. Priolo, Spectral element method for acoustic wave simulation in heterogeneous media, Finite elements in analysis and design 16 (3) (1994) 337–348.

[8] D. Komatitsch, S. Tsuboi, J. Tromp, The spectral-element method in seismology, in: A. Levander, G. Nolet (Eds.), Seismic Earth: Array Analysis of Broadband Seismograms, Vol. 157 of Geophysical Monograph, American Geophysical Union, 2005, pp. 205–228.

[9] E. Casarotti, M. Stupazzini, S. J. Lee, D. Komatitsch, A. Piersanti, J. Tromp, CUBIT and seismic wave propagation based upon the spectral-element method: an advanced unstructured mesher for complex 3D geological media, in: M. L. Brewer, D. Marcum (Eds.), Proceedings of the 16th International Meshing Roundtable, no. 5B, Springer, 2008, pp. 579–597.

[10] P. Cupillard, E. Delavaud, G. Burgos, G. Festa, J.-P. Vilotte, Y. Capdeville, J.-P. Montagner, RegSEM: a versatile code based on the spectral element method to compute seismic wave propagation at the regional scale, Geophysical Journal International 188 (3) (2012) 1203–1220.

[11] K. C. Meza Fajardo, Numerical simulation of wave propagation in unbounded elastic domains using the spectral element method, Ph.D. thesis, Università degli Studi di Pavia, Italy (2007).

[12] D. Komatitsch, J.-P. Vilotte, R. Vai, J. M. Castillo-Covarrubias, F. J. Sánchez-Sesma, The spectral element method for elastic wave equations – application to 2-D and 3-D seismic problems, International Journal for Numerical Methods in Engineering 45 (9) (1999) 1139–1164.

[13] I. Mazzieri, M. Stupazzini, R. Guidotti, C. Smerzini, SPEED: SPectral Elements in Elastodynamics with Discontinuous Galerkin: a non-conforming approach for 3D multi-scale problems, International Journal for Numerical Methods in Engineering 95 (12) (2013) 991–1010.

[14] A. T. Patera, A spectral element method for fluid dynamics: laminar flow in a channel expansion, Journal of Computational Physics 54 (3) (1984) 468–488.

[15] G. Karniadakis, S. Sherwin, Spectral/hp element methods for computational fluid dynamics, Oxford University Press, 2013.

[16] R. J. LeVeque, Wave propagation algorithms for multidimensional hyperbolic systems, Journal of Computational Physics 131 (2) (1997) 327–353.

[17] L. Fezoui, S. Lanteri, S. Lohrengel, S. Piperno, Convergence and stability of a discontinuous Galerkin time-domain method for the 3D heterogeneous Maxwell equations on unstructured meshes, ESAIM: Mathematical Modelling and Numerical Analysis 39 (6) (2005) 1149–1176.

[18] T. Nagell, Introduction to number theory, Wiley, 1951.

[19] N. Tordjman, Éléments finis d'ordre élevé avec condensation de masse pour l'équation des ondes, Ph.D. thesis, Université Paris IX-Dauphine, Paris, France (1995).

[20] S. Fauqueux, Modélisation de la propagation d'ondes en milieu élastique par éléments finis mixtes avec condensation de masse, Ph.D. thesis, Université Paris IX-Dauphine, Paris, France (2003).

[21] M. Shinozuka, G. Deodatis, Simulation of stochastic processes by spectral representation, Applied Mechanics Reviews 44 (4) (1991) 191–205.

Appendix A. Solutions of Equation (63)

The three classes of solutions of Equation (63) and their relevance to the stability of the Leap-Frog scheme are discussed in this Appendix.

Appendix A.1. Solutions corresponding to $\omega = 0$

Introducing $\omega = 0$ into the characteristic polynomial of Equation (62), the following cubic equation is obtained

$$\lambda_l^3 - 90A_1\lambda_l^2 + 1800\beta^2\lambda_l = 0, \tag{A.1}$$

whose solutions are

$$\chi_1 = 0, \quad \chi_2 = 15\left(3A_1 + \sqrt{9A_1^2 - 8\beta^2}\right), \quad \chi_3 = 15\left(3A_1 - \sqrt{9A_1^2 - 8\beta^2}\right). \tag{A.2}$$

Using the definition of the parameters A_1 and β, and after algebraic manipulations, it can be shown that the condition $9A_1^2 - 8\beta^2 > 0$ is equivalent to

$$\frac{(\gamma_i + \gamma_{i,1})^2}{\eta_i\eta_{i,2}} + \frac{(\gamma_i + \gamma_{i,2})^2}{\eta_i\eta_{i,1}} + \frac{(3\gamma_i + \gamma_{i,1})^2}{5\eta_{i,2}^2} + \frac{(3\gamma_i + \gamma_{i,2})^2}{5\eta_{i,1}^2} + \frac{8\gamma_i^2}{5\eta_{i,1}\eta_{i,2}} + \frac{5}{4\eta_i^2}\left((2\gamma_i + \gamma_{i,1})^2 + 4\gamma_i\gamma_{i,2} + 2\gamma_{i,1}\gamma_{i,2} + \gamma_{i,2}^2\right) > 0 \tag{A.3}$$

which is clearly satisfied for any choice of the material parameters. Therefore, the three solutions in Equation (A.2) are always real. More importantly, the maximum of the three solutions is always attained by χ_2, meaning that this is the only relevant solution for the stability of the Leap-Frog scheme.

Appendix A.2. Solutions corresponding to $\omega^2 = 1$

Introducing $\omega^2 = 1$ into the characteristic polynomial of Equation (62), the following cubic equation is obtained

$$\lambda_l^3 - 3\sigma_1(1)\lambda_l^2 + 6\sigma_2(1)\lambda_l - 2\sigma_3(1) = 0, \tag{A.4}$$

and the three roots are

$$\chi_4 = \tau_1 + \tau_3 + \frac{\tau_2}{\tau_3}, \tag{A.5}$$

$$\chi_5 = \tau_1 - \frac{1}{2}\left(\tau_3 + \frac{\tau_2}{\tau_3}\right) + \frac{\sqrt{3}}{2}\left(\tau_3 - \frac{\tau_2}{\tau_3}\right) I, \tag{A.6}$$

$$\chi_6 = \tau_1 - \frac{1}{2}\left(\tau_3 + \frac{\tau_2}{\tau_3}\right) - \frac{\sqrt{3}}{2}\left(\tau_3 - \frac{\tau_2}{\tau_3}\right) I, \tag{A.7}$$

where $\tau_i = \sigma_i(1)$ for $i = 1, 2, 3$.

From the definitions in Equations (48) and (49), it is clear that τ_1 and τ_2 are real, whereas τ_3 can be real or complex.

If τ_3 is real, then χ_4 is real and χ_5 and χ_6 are complex. In this case only χ_4 is relevant from the point of view of the stability of the Leap-Frog scheme.

If τ_3 is complex then it can be shown that $\tau_2 = |\tau_3|^2$ by using Equation (49). This implies that χ_4, χ_5 and χ_6 are real and they can be rewritten as

$$\chi_4 = \tau_1 + 2\Re\{\tau_3\}, \tag{A.8}$$

$$\chi_5 = \tau_1 - \Re\{\tau_3\} - \sqrt{3}\Im\{\tau_3\}, \tag{A.9}$$

$$\chi_6 = \tau_1 - \Re\{\tau_3\} + \sqrt{3}\Im\{\tau_3\}, \tag{A.10}$$

It is possible to prove that χ_4 is always the maximum of the three roots and therefore it is the only relevant from the point of view of the stability of the Leap-Frog scheme. Using the polar representation of a complex number, τ_3 can be written as $\tau_3 = \sqrt{\tau_2}[\cos(\theta) + i\sin(\theta)]^{1/3}$ where $\tan(\theta) = \sqrt{\tau_2^3 - \tau^2}/\tau$. It is worth noting that $\tau_2^3 - \tau^2 > 0$ because of the assumption of τ_3 being complex.

The application of the De Moivre's theorem [18] leads to

$$\Re\{\tau_3\} = \sqrt{\tau_2}\cos(\theta/3), \qquad \Im\{\tau_3\} = \sqrt{\tau_2}\sin(\theta/3). \tag{A.11}$$

Finally, it can be observed that, if $\theta \in [0, \pi)$, then $\Im\{\tau_3\} > 0$. This clearly implies that $\chi_6 > \chi_5$. More importantly, $\theta \in [0, \pi)$ leads to $3\Re\{\tau_3\} > \sqrt{3}\Im\{\tau_3\}$, which is equivalent to $\chi_4 > \chi_6$. An analogous argument can be used to prove that $\chi_4 > \chi_5 > \chi_6$ when $\theta \in (-\pi, 0]$. It is worth mentioning that the case $\theta = \pi$ corresponds to τ_3 being real.

Appendix A.3. Solutions corresponding to the roots of the polynomial T

The number of real roots of the polynomial T depends upon the parameters δ_1 and δ_2. If $\delta_1 \neq 0$ the two roots of T are real, namely $-30(\delta_2 \pm \sqrt{\delta_2^2 - 2\beta^2\delta_1})/\delta_1$. If $\delta_1 = 0$ and $\delta_2 \neq 0$, there is only one real root, that is $-30\beta^2/\delta_2$. Finally, if $\delta_1 = \delta_2 = 0$, T has no real roots.

Introducing $\lambda_l = -30(\delta_2 \pm \sqrt{\delta_2^2 - 2\beta^2\delta_1})/\delta_1$ in Equation (62) leads to

$$\left(\delta_2 \pm \sqrt{\delta_2^2 - 2\beta^2\delta_1}\right)(2\delta_2 + 3A_1\delta_1) + 2\beta^2\delta_1(\delta_1 - 1) = 0, \tag{A.12}$$

provided that $\delta_1 \neq 0$. Analogously, introducing $\lambda_l = -30\beta^2/\delta_2$ in Equation (62) leads to

$$\beta^2 + \delta_2(3A_1 + 2\delta_2) = 0, \tag{A.13}$$

provided that $\delta_1 = 0$ and $\delta_2 \neq 0$.

From Equation (62), it is clear that the solutions corresponding to the roots of T correspond to the solutions described in Appendix A.1 (i.e. when $\omega = 0$) with extra restrictions on the material parameters given by Equations (A.12) and (A.13). Therefore, the solutions corresponding to the roots of the polynomial T are already included by the solutions given by Equation (A.2).

Appendix A.4. Positivity of the solutions χ_2 and χ_4

The positivity of the two solutions relevant to the stability of the Leap-Frog scheme, namely χ_2 and χ_4, is discussed next. The positivity of χ_2 is clear as $\beta > 0$, $A_1 > 0$ and, as previously discussed, $9A_1^2 - 8\beta^2 > 0$.

In order to discuss the positivity of χ_4, two cases are considered. If τ_3 is complex, it is possible to show that $\chi_4 = \tau_1 + 2\Re\{\tau_3\} > 0$ because $\tau_1 > 0$ and $\cos(\theta/3) > 0, \forall\theta \in (-\pi, \pi)$. It is worth noting that the condition $\tau_1 > 0$ is equivalent to

$$\frac{49\gamma_i}{5\eta_i} + \frac{\gamma_{i,1} + \gamma_{i,2}}{2\eta_i} + \frac{3\gamma_i + \gamma_{i,1}}{\eta_{i,2}} + \frac{3\gamma_i + \gamma_{i,2}}{\eta_{i,1}} > 0, \tag{A.14}$$

which is clearly satisfied for any combination of the material parameters. Finally, if τ_3 is real it is easy to show that $\tau_1 + \tau_3 + \frac{\tau_2}{\tau_3} > 0$ because it is the maximum root and the polynomial P of Equation (62) satisfies that $P(0) < 0$ and $\lim_{\lambda_l \to \infty} P(\lambda_l) > 0$.